

## Model for diffusion on deformable lattices. I. Collective diffusion

T. Ala-Nissila,\* J. Kjoll, and S. C. Ying

*Department of Physics, Brown University, Providence, Rhode Island 02912*

R. A. Tahir-Kheli

*Institut Max von Laue-Paul Langevin, Centre de Tri, avenue des Martyrs, Boîte Postale 156X,  
38042 Grenoble CEDEX, France*

*and Department of Physics, Temple University, Philadelphia, Pennsylvania 19122*

(Received 26 November 1990)

We present results of theoretical calculations of collective diffusion in a lattice-gas model of a deformable lattice, which has been proposed to explain the anomalous-diffusion anisotropy of adatoms on a deformable lattice, such as H on W(110). This model contains a competition between intercell and intracell diffusion jumps. The latter occur through a barrier created by a local distortion of the underlying substrate. The central parameter of the model is the branching ratio  $r$ , which is defined as the ratio of intracell-to-intercell diffusion rates. We perform extensive Monte Carlo random-walk simulations of diffusion as a function of coverage for several values of  $r$ , for a model including only intracell hard-core interactions. Using the Green's-function method, we obtain an analytic mean-field solution for the diffusion tensor. We also present the derivation of a higher-order solution in the Green's-function expansion. We study the validity of the analytic solutions by comparison with the simulations. Finally, we remark on the relevance of our results to diffusion experiments for H/W(110).

### I. INTRODUCTION

Perhaps the simplest example of a diffusive process consists of classical particles executing isotropic random walks on an inert lattice. In the case of only one particle, the corresponding diffusion constant can trivially be written down as  $Ia^2/z$ , where  $z$  is the coordination number of the lattice,  $I$  is the jump rate, and  $a$  the lattice constant (i.e., the length of each jump).<sup>1</sup> However, in the presence of other particles, the diffusion process becomes correlated and nontrivial.<sup>2</sup> Additionally, a distinction has to be made between single particle or tracer and collective- or chemical-diffusion processes. The interparticle correlations play a particularly important role in two-dimensional systems. A substantial amount of analytic work and numerical simulations have been done in simple lattice-gas systems in order to study these correlation effects as a function of the coverage  $c$  ( $0 \leq c \leq 1$ ).<sup>1-3</sup> So far, complete analytic solutions for all coverages exist only in cases where interactions between particles can be neglected, except for the double-occupancy or site-exclusion hard-core interaction.<sup>2,3</sup> Most of the current work has concentrated on tracer diffusion, since with only an on-site hard-core interaction present the collective-diffusion tensor is independent of coverage,<sup>4</sup> while tracer diffusion shows complicated dependence on  $c$ .<sup>2,3</sup>

Surface diffusion of adatoms on a substrate<sup>5</sup> provides an important realization of classical diffusion in two dimensions, which has frequently been modeled by lattice-gas systems.<sup>2,6-8</sup> However, in reality, the adsorption of an adatom is often accompanied by a local substrate relaxation or distortion.<sup>5-10</sup> Recently, it has been proposed that this local distortion can have significant effect

on the surface-diffusion tensor.<sup>6-9</sup> A novel lattice-gas model was introduced which incorporates the essence of such a distortion with respect to diffusion.<sup>7</sup> This model has been proposed to explain the observed diffusion anisotropy of H adatoms on a W(110) surface.<sup>8</sup> The essence of the model is to recognize that the binding energy of a H adatom can be lowered if it is displaced locally from the original adsorption site along the  $(1\bar{1}0)$  direction and accompanied by the shift of surrounding substrate atoms in the same direction (see Fig. 1). Obviously, the same is true if the displacements of both the adatom and surrounding substrate atoms are reversed. This results in a "dynamical" double-well-type adsorption potential, which is imposed on the surface unit cell by each diffusing particle. When these distortions start to correlate mutually for higher coverages, a global surface reconstruction may occur, such as has been observed for H on W(110) around  $c \approx 0.5$ .<sup>10</sup>

An important feature of the model is that, even without direct adatom interactions, double occupation of an adsorption site is not favorable. This happens because of the opposing substrate distortions of two adatoms within the same cell that leads to a large local increase in the energy. Since the time scale for the adatom motion is much longer than a typical time scale for the substrate response, the effect just described can be approximately modeled by splitting the original single adsorption site into *two* symmetric sites. When this is done, an energy barrier exists for the motion from one subsite to another. Moreover, a simultaneous occupation of the two subsites is then forbidden; i.e., the hard-core repulsion applies within each *cell*. In the context of a simple random-walk theory, the diffusive motion of the adatoms can then be considered to consist of two separate steps on a static lat-

tice. The first is an *intracell* jump across the barrier originating from the local distortion, while the second is an *intercell* jump across the barrier due to the usual periodic arrangement of the substrate atoms. The competition between these two processes can be parametrized by a

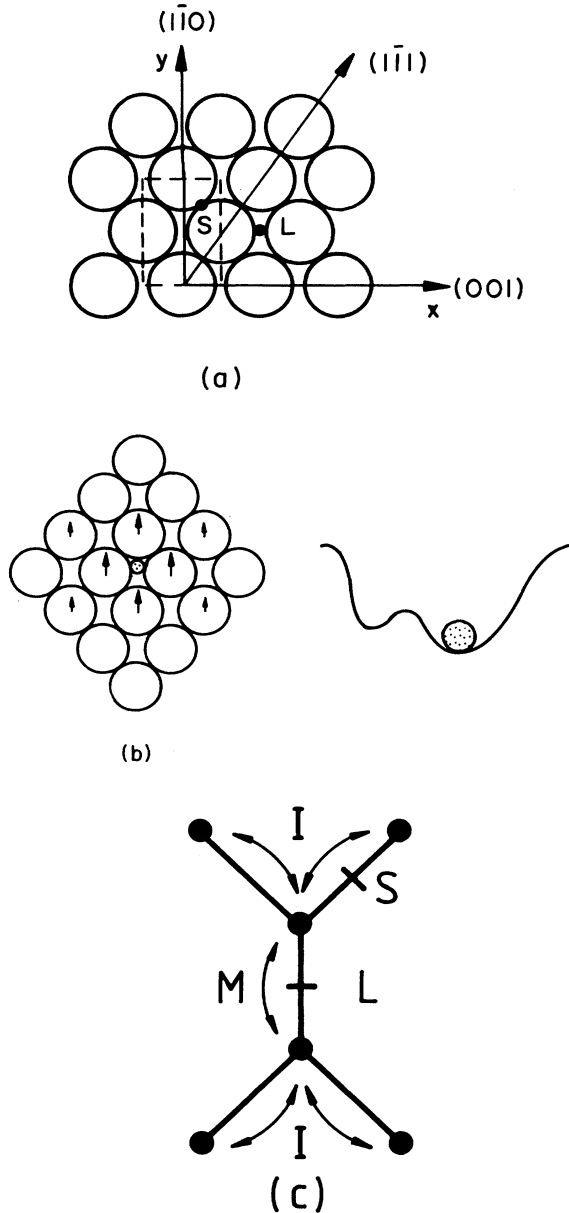


FIG. 1. (a) Geometry of an undistorted W(110) surface (from Ref. 7). The hourglass adsorption sites of adatoms (cells) are denoted by  $L$ , while  $S$  denotes the saddle points of the surface potential. (b) A schematic figure of a local distortion caused by an adsorbed H adatom (shaded circle) (Ref. 7). Arrows denote the displacements of the outmost atomic layer, which causes a local symmetry breaking of the hourglass sites. (c) A simplified lattice-gas model or diffusion which takes into account the effect of the distortion. Each hourglass now contains two equivalent sites, denoted by circles. Diffusion consists of two steps, namely, intracell jumps with rate  $M$  and intercell jumps with rate  $I$ .

*branching ratio*  $r$ , which is the ratio of the intracell-to-intercell diffusion rates. In realistic adsorption systems, additional direct or indirect interactions exist between adatoms on different adsorption sites, as evidenced by the appearance of many distinct ordered phases of the adlayer.<sup>10</sup> However, even without these interactions, the presence of both intracell and intercell jumps as well as the exclusion of double occupancy within a cell already leads to a very complicated coverage dependence and causes strong correlation effects to appear for both tracer and collective diffusion in the model. Having said this, a note of caution must also be added: The assumption of a static substrate renders the model physically applicable for H/W(110) only in the regime where no global reconstruction of the substrate occurs.

To explore fully the effects of a local lattice distortion on diffusion, we have undertaken a comprehensive study of the collective-diffusion process within our lattice-gas model. In this paper we shall concentrate on the case of a hard-core repulsion which applies to *both* sites in a given cell. This implies a strict exclusion of a double occupancy in each cell. The behavior of the tracer-diffusion tensor under the same constraint, as well as the effect of full adatom interactions, is planned to be presented in other subsequent publications.<sup>11,12</sup>

We start this work by presenting results of extensive Monte Carlo random-walk simulations as a function of coverage for various values of the branching ratio  $r$ . These results extend and generalize the earlier study of Kjoll, Ala-Nissila, and Ying<sup>7</sup> for  $r=3$ . Our results demonstrate how the diffusion anisotropy depends on coverage and  $r$ . Using the Green's-function method, we then construct an analytic mean-field solution for the collective-diffusion tensor  $D$ . This solution turns out to be moderately accurate for  $r \gtrsim 1$ , in particular as far as the behavior of the diffusion anisotropy  $D_{yy}/D_{xx}$  is concerned. Additionally, in the limit  $r \rightarrow \infty$ , it reduces correctly to the trivial, coverage-independent solution. We also construct an improved solution by including some of the higher-order terms beyond mean-field theory. This leads to a set of self-consistent equations, which we solve numerically for all coverages as a function of  $r$ . Next, we present comparisons of these two solutions with the results obtained from Monte Carlo simulations. Finally, we remark on the relevance of our results to experiments on the H/W(110) system.

## II. MONTE CARLO SIMULATIONS OF COLLECTIVE DIFFUSION

As discussed in the Introduction, the physical motivation behind the diffusion model introduced by Kjoll, Ala-Nissila, and Ying<sup>7</sup> is based on the anomalous-diffusion anisotropy of H adatoms on a W(110) surface.<sup>8</sup> On an ideal surface, the underlying surface forms a centered rectangular lattice, with adatoms adsorbed on the long bridge sites within the "hourglass" potential [see Fig. 1(a)]. The principal axes of diffusion are given by the (110) and (001) directions denoted by  $y$  and  $x$ , respectively. When H is adsorbed on the surface, this local symmetry is broken by a uniform shift of the adatoms [Fig.

1(b)]. Thus, within a random-walk picture, we describe the diffusion problem by a *two-step lattice-gas model* with jump rates  $M$  and  $I$  for intracell and intercell rates, respectively, as shown in Fig. 1(c). The branching ratio  $r = I/M$  then determines the value of the diffusion anisotropy, which, in the zero coverage limit, is given exactly by<sup>7</sup>

$$\frac{D_{yy}}{D_{xx}} = \frac{r}{r+2} \left( \frac{b}{a} \right)^2. \quad (2.1)$$

Here  $a$  and  $b$  denote the dimensions of the underlying unit cell, and for the W(110) surface,  $(b/a)^2 = 2$ . By symmetry, the off-diagonal terms  $D_{xy} = D_{yx} = 0$ . In the limit  $r \rightarrow \infty$ , the effect of the local distortion vanishes and the diffusion anisotropy (2.1) recovers the ideal surface value of  $D_{yy}/D_{xx} = 2$  for W(110). The same result applies in the limit  $c \rightarrow 1$ , where blocking of intercell jumps by occupied neighboring cells drives the effective branching ratio to infinity.<sup>7</sup> However, for any finite value of  $r$  and  $c < 1$ , the anisotropy ratio is always less than 2 in accordance with experiments of H diffusion.<sup>8</sup> The parameter  $r$ , which we treat as a constant here, obviously has complicated temperature and coverage dependence arising from microscopic interactions, which cannot be incorporated into a lattice-gas model. However, as recent microscopic calculations of diffusion of single particles in locally distorted potentials have shown,<sup>9</sup> Eq. (2.1) nevertheless gives qualitatively correct behavior for the anisotropy in the limit where temperature is low compared to the classical saddle-point barriers.

Preliminary results of Kjoll, Ala-Nissila, and Ying<sup>7</sup> have shown that for  $r = 3$ , the diffusion anisotropy is a relatively slowly varying function of coverage. To extend and generalize their study, we have performed extensive Monte Carlo (MC) random-walk simulations as a function of coverage for several values of the branching ratio  $r$ . We assume no direct adatom-adatom interactions except for the in-cell exclusion within each hourglass. To obtain the elements of the diffusion tensor  $D_{yy}$  and  $D_{xx}$ , we have computed the density-fluctuation autocorrelation function<sup>7,13</sup>

$$S(\mathbf{R}, \mathbf{R}', t) = \langle \delta n(\mathbf{R}, t) \delta n(\mathbf{R}', 0) \rangle, \quad (2.2)$$

where the spontaneous density fluctuations are given by  $\delta n(\mathbf{R}, t) = n(\mathbf{R}, t) - \langle n(\mathbf{R}, t) \rangle$ . In the hydrodynamic regime, the Fourier transform of this correlation function decays as

$$s(\mathbf{k}, t) = S(\mathbf{k}, 0) e^{-\mathbf{k} \cdot \mathbf{D} \cdot \mathbf{k} t}. \quad (2.3)$$

This allows us to extract the elements of  $\mathbf{D}$  by choosing  $\mathbf{k}$  along the  $x$  and  $y$  axes. In our simulations we have first computed the sine and cosine transforms of the density fluctuations separately and then added the corresponding correlation functions together to reduce noise.

To study finite-size behavior, we have used systems of sizes  $30 \times 30$ ,  $60 \times 60$ , and  $100 \times 100$ , with fully periodic boundary conditions. Most of the results presented here are for  $60 \times 60$  lattices. Usually, the spontaneous fluctuations of density were large enough so that only times up to few hundred MC steps per particle were needed in cal-

culating (2.3), and no auxiliary driving force was employed. Particular care was taken to ensure that the simulations had reached the proper hydrodynamic regime by using two of the smallest possible values of  $k_x$  and  $k_y$  in computing  $S(\mathbf{k}, t)$  and verifying that the higher-order corrections in  $\mathbf{k}$  were negligible. We usually performed about  $10^3$ – $10^4$  consecutive runs over the chosen time interval to obtain reliable configuration averages. Additionally, to ensure that the initial configurations for each run at  $t = 0$  were independent, we use a thermalization subroutine between each run. This routine randomizes each initial configuration. This

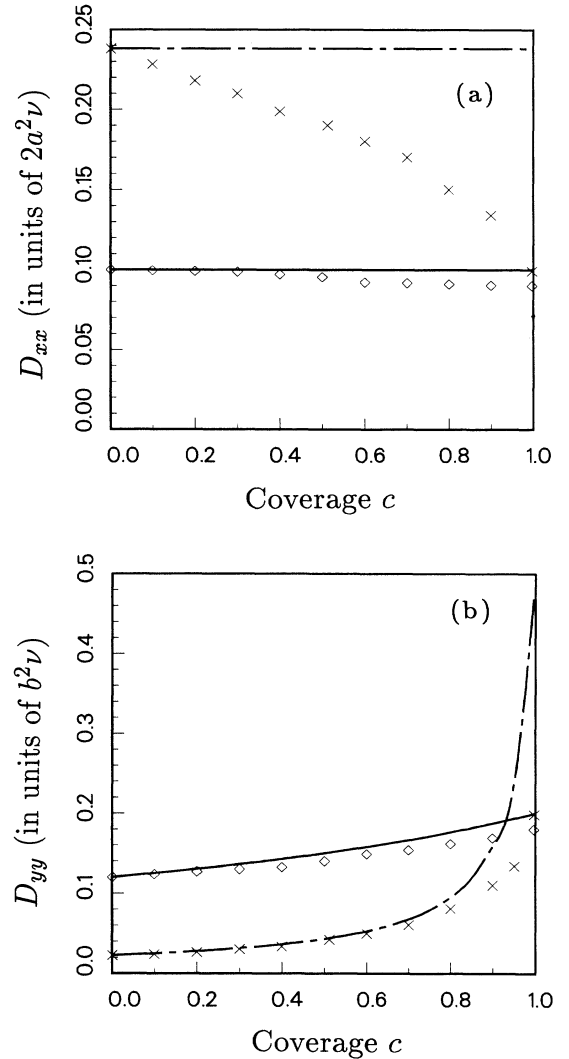


FIG. 2. Results of MC simulations for the model of collective diffusion on the W(110) surface, where  $2a^2 = b^2$ . The magnitude of the overall rate coefficient  $\nu$  is arbitrary. (a)  $D_{xx}$  vs coverage for branching ratios  $r = 3$  (diamonds) and  $r = \frac{1}{10}$  (crosses). For comparison, the MF results of Sec. III A are also shown (solid line for  $r = 3$ , and dashed line for  $r = \frac{1}{10}$ ). (b)  $D_{yy}$  for  $r = 3$  (diamonds for MC and solid line for MF) and  $r = \frac{1}{10}$  (crosses for MC and dashed line for MF). The error bars for MC results are smaller than the sizes of the points.

proved to be important for higher coverages and small values of the branching ratio. Our results and test runs showed virtually no noticeable finite-size effects beyond systems of the size  $30 \times 30$  within our statistics.

In Fig. 2 we show results of our simulations for two branching ratios  $r=0.1$  and 3, corresponding to the geometry for the W(110) surface of Fig. 1. First,  $D_{xx}$ , which is shown in Fig. 2(a), is a relatively slowly varying function of coverage for branching ratios  $r \gtrsim 1$ . For  $r=3$  it is already rather close to the coverage-independent limit of  $r \rightarrow \infty$ .  $D_{yy}$  shows stronger coverage dependence even for  $r=3$  evident in Fig. 2(b). However, for both quantities the correlation effects remain rather weak for  $c \lesssim 0.5$ , which indicates that Eq. (2.1) is a relatively good approximation of the anisotropy ratio for these branching ratios. To understand the nature of these correlation effects, in the next section we will develop an analytic theory to calculate  $D$ .

### III. GREEN'S-FUNCTION METHOD FOR COLLECTIVE DIFFUSION AT ALL COVERAGES

In the presence of more than one particle, the in-cell hard-core interactions cause nontrivial particle-particle correlations to appear, as we have seen in the MC results. In the case of only a single-site hard-core interaction, it can be shown rigorously for collective diffusion that these correlations cancel out and the single-particle random-walk results apply for all coverages  $c < 1$ .<sup>4</sup> However, the additional hourglass site exclusion of the two-step model being considered here invalidates this simple result. To calculate the effect of correlations for the case of tracer diffusion, an equation-of-motion method based on Green's-function formalism has been developed by Tahir-Kheli and Elliott<sup>14</sup> (TKE) and further refined by Tahir-Kheli and others.<sup>15-17</sup> The TKE method has been applied with very good results to a variety of lattice-gas systems, where only the on-site blocking interaction is present.<sup>3</sup> Within the TKE method, one derives a formally exact equation of motion for the frequency- and wave-vector-dependent fluctuation correlation Green's function, which then can be solved using various decoupling schemes. This method can be generalized to treat the case of collective diffusion as well, as we use it below to derive an analytic solution of  $D$  for our lattice-gas model.

Let us consider diffusion on the somewhat more general lattice-gas model of Fig. 3 with two distinct sublattices  $A$  and  $B$  in a given unit cell. In addition to the single-site hard-core exclusion, we shall impose the condition that only one of these sublattice sites can be simultaneously occupied. Clearly, each cell of this generalized model then corresponds to the hourglass adsorption sites of our surface model. Let  $n(t)$  denote a stochastic occupancy variable of the diffusing particles, which are all assumed to be identical. If at a time  $t$  a particle is on sublattice  $A$  in cell (i.e., the hourglass) labeled  $g$ , then  $n_g^A(t)=1$ ; otherwise,  $n_g^A(t)=0$ . A corresponding definition  $n_g^B(t)$  is adopted for a particle on sublattice  $B$ . Using these variables, we can write an exact rate equation for a particle occupying sublattice  $A$  in cell  $g$ :

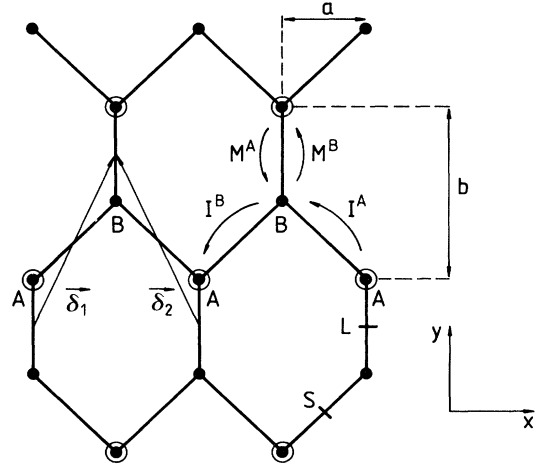


FIG. 3. Geometry of the generalized two-step model which is used for the theoretical calculations of Sec. III. Diffusion rates and concentration of particles on sublattices  $A$  (circled dots) and  $B$  (dots) can be different, as discussed in the text. The vectors  $\delta_1$  and  $\delta_2$  connecting periodic cells are also shown schematically.  $L$  and  $S$  refer to the original surface model of Fig. 1.

$$\begin{aligned} \frac{d}{dt} n_g^A(t) = & -M^A n_g^A(t) + M^B n_g^B(t) \\ & - \sum_f I^A(gf) n_g^A(t) [1 - n_f^B(t) - n_f^A(t)] \\ & + \sum_f I^B(fg) n_f^B(t) [1 - n_g^A(t) - n_g^B(t)]. \end{aligned} \quad (3.1)$$

The corresponding equation for a particle on sublattice  $B$  can simply be obtained by interchanging  $A$  and  $B$  in (3.1). Here  $M^A$  is the intracell jump rate associated with the particle hopping from sublattice  $A$  to sublattice  $B$  within the hourglass, while  $M^B$  is the rate for a jump in the opposite direction.  $I^A(gf)$  and  $I^B(gf)$  are hopping rates associated with an intercell jump from cell  $g$  to cell  $f$  originating from either  $A$  or  $B$  sublattice, respectively. We restrict ourselves to the case where only nearest-neighbor jumps are allowed, i.e.,  $I^A(gf)=I^A$ , when  $f-g=\delta_1$  or  $\delta_2$ , and is zero otherwise, whereas  $I^B(gf)=I^B$  for  $f-g=-\delta_1$  or  $-\delta_2$ , and zero otherwise. Here  $\delta_1=(a,b)$  and  $\delta_2=(-a,b)$  denote vectors connecting the lattice periodically from one hourglass to another (see Fig. 3).

The occupancy variables can be written in terms of the fluctuations in the stochastic occupancy variables and the coverage on the specified sublattice as  $n_g^S(t)=u_g^S(t)+c^S$ . (To simplify the notation, from here on we use the superscript  $S$  to denote  $A$  or  $B$ , while  $SS'$  can be any of the four combinations  $AA$ ,  $AB$ ,  $BA$ , or  $BB$ .) The statistical averages of  $n_g^A(t)$  and  $n_g^B(t)$  denoted by  $c^A$  and  $c^B$  are the coverages on sublattices  $A$  and  $B$ , respectively. The total coverage  $c=c^A+c^B$  is the sum of the coverages on the two sublattices, which, for convenience, is normalized to unity corresponding to the maximum allowed occupancy of one particle in each hourglass.

Given the rate equations for the particle fluctuations, the TKE method consists of finding an equation of motion for the retarded Green's functions of the fluctuation correlated functions. From the solution of these equations, we can then extract the elements of the diffusion tensor from the pole of the Green's functions. To this end we first define the retarded density-density-fluctuation Green's function. It refers to the probability that when a fluctuation on the  $A$  sublattice of cell  $g$ 's is present at  $t=0$ , another fluctuation at sublattice  $S$  of cell  $g$  will occur at a later time  $t$ :

$$\begin{aligned} G_{gg'}^S(t) &= -2\pi i \theta(t) \langle u_g^S(t) u_{g'}^A(0) \rangle \\ &\equiv \langle \langle u_g^S(t); u_{g'}^A(0) \rangle \rangle, \end{aligned} \quad (3.2)$$

where  $\theta(t)$  is the Heaviside step function,

$$\theta(t) = \begin{cases} +1, & \text{for } t > 0 \\ 0, & \text{otherwise.} \end{cases} \quad (3.3)$$

We also need the four next-higher-order Green's functions which refer to triple density fluctuations:

$$G_{gg'}^{SS'}(t) = \langle \langle u_g^S(t) u_{g'}^{S'}(t); u_{g'}^A(0) \rangle \rangle. \quad (3.4)$$

To derive the equation of motion for  $G_{gg'}^S(t)$ , we use the rate equations (3.1). This gives

$$\begin{aligned} \frac{d}{dt} G_{gg'}^S(t) &= -2\pi i \delta(t) \langle u_g^S(t) u_{g'}^A(0) \rangle \\ &\quad - 2\pi i \theta(t) \left\langle \left[ \frac{d}{dt} u_g^S(t) \right] u_{g'}^A(0) \right\rangle. \end{aligned} \quad (3.5)$$

The first term on the right-hand side is an equal-time term which results from the time derivative of the Heaviside function. Using the result that  $(n_g^S)^2 = n_g^S$  and  $n_g^S n_g^{S'} = 0$  for  $S \neq S'$ , we obtain the result  $\langle u_g^A(t) u_{g'}^A(0) \rangle = \delta_{gg'} c^A (1 - c^A)$  for  $S = A$  and  $\langle u_g^B(t) u_{g'}^A(0) \rangle = -\delta_{gg'} c^A c^B$  for  $S = B$ . As mentioned above, the second term is calculated by inserting the equation of motion (3.1), which in turn leads to terms involving the higher-order Green's functions (3.4).

To proceed further we next define the Fourier transforms of the Green's functions in frequency and reciprocal space as

$$G_{gg'}^S(\omega) = \frac{1}{N} \int_{-\infty}^{\infty} d\omega \sum_{\mathbf{k}} G_{\mathbf{k}}^S(\omega) e^{-i\omega t} e^{i\mathbf{k} \cdot (\mathbf{g} - \mathbf{g}')} \quad (3.6)$$

and

$$\begin{aligned} G_{gg'}^{SS'}(\omega) &= \frac{1}{N^2} \int_{-\infty}^{\infty} d\omega \sum_{\mathbf{k}_1, \mathbf{k}_2} G_{\mathbf{k}_1 \mathbf{k}_2}^{SS'}(\omega) e^{-i\omega t} \\ &\quad \times e^{i\mathbf{k}_1 \cdot (\mathbf{g} - \mathbf{g}') + i\mathbf{k}_2 \cdot (\mathbf{1} - \mathbf{g}')}. \end{aligned} \quad (3.7)$$

The corresponding Fourier transforms for the jump rates are

$$J^S(\mathbf{q}) = \sum_{\mathbf{g}-\mathbf{f}} I^S(\mathbf{g}\mathbf{f}) e^{-i\mathbf{q} \cdot (\mathbf{g} - \mathbf{f})}. \quad (3.8)$$

Using these definitions, we arrive at the following equations of motion for the density-density Green's functions:

$$\begin{aligned} [-i\omega + \beta^A(\mathbf{k})] G_{\mathbf{k}}^A &= -ic^A(1 - c^A) + \alpha^B(\mathbf{k}) G_{\mathbf{k}}^B \\ &\quad + I^A \sum_{\delta} [\rho_{\mathbf{k}}^{AA}(\delta) + \rho_{\mathbf{k}}^{AB}(\delta)] \\ &\quad - I^B \sum_{\delta} e^{i\mathbf{k} \cdot \delta} [\rho_{\mathbf{k}}^{BB}(-\delta) + \rho_{\mathbf{k}}^{BA}(-\delta)] \end{aligned} \quad (3.9)$$

and

$$\begin{aligned} [-i\omega + \beta^B(\mathbf{k})] G_{\mathbf{k}}^B &= ic^A c^B + \alpha^A(\mathbf{k}) G_{\mathbf{k}}^A \\ &\quad + I^B \sum_{\delta} [\rho_{\mathbf{k}}^{BB}(-\delta) + \rho_{\mathbf{k}}^{BA}(-\delta)] \\ &\quad - I^A \sum_{\delta} e^{-i\mathbf{k} \cdot \delta} [\rho_{\mathbf{k}}^{AA}(\delta) + \rho_{\mathbf{k}}^{AB}(\delta)]. \end{aligned} \quad (3.10)$$

Here the sum over  $\delta$  covers both  $\delta_1$  or  $\delta_2$ . We have also suppressed the explicit frequency dependence of the Green's functions for simplicity. The quantities  $\alpha^S(\mathbf{k})$  and  $\beta^S(\mathbf{k})$  are defined by

$$\alpha^S(\mathbf{k}) = M^S + vJ^S(-\mathbf{k}) - c^S J^S(0) + c^{S'} J^{S'}(\mathbf{k}) \quad (3.11)$$

and

$$\beta^S(\mathbf{k}) = M^S + vJ^S(0) + c^{S'} J^{S'}(0) - c^S J^S(\mathbf{k}), \quad (3.12)$$

where  $S, S'$  denotes  $A, B$  or  $B, A$ . The quantity  $\rho_{\mathbf{k}}^{SS'}(\delta)$  which depends on  $\mathbf{k}$  and  $\delta$  is defined by the expression

$$\rho_{\mathbf{k}}^{SS'}(\delta) = \frac{1}{N} \sum_{\mu} G_{\mathbf{k}-\mu, \mu}^{SS'} e^{i\mu \cdot \delta}. \quad (3.13)$$

Using the identity  $G_{gg'}^{SS'}(t) = G_{gg'}^{S'S}(t)$ , we are led to the important symmetry relation

$$\rho_{\mathbf{k}}^{SS'}(\delta) = e^{i\mathbf{k} \cdot \delta} \rho_{\mathbf{k}}^{S'S}(-\delta), \quad (3.14)$$

where  $\delta$  can be either  $\delta_1$  or  $\delta_2$ . The symmetry relations play an important role in the analytic theory of Sec. III B. It should be mentioned, however, that in obtaining Eqs. (3.9) and (3.10) we have also used the detailed balance conditions

$$c^A M^A = c^B M^B \quad (3.15)$$

and

$$c^A J^A(0) = c^B J^B(0). \quad (3.16)$$

Hence the diffusion rates  $M^A$ ,  $M^B$ ,  $J^A(0)$ , and  $J^B(0)$  are not all independent parameters, but are constrained by the relations (3.15) and (3.16).

In order to obtain a complete solution for the Green's functions  $G^S$  in Eqs. (3.9) and (3.10), one has to solve for the quantities  $\rho_{\mathbf{k}}^{SS'}$ . The equation of motion for the Green's functions  $G^{SS'}$  contained in them in turn depends on yet higher-order Green's functions through an infinite hierarchy of equations. However, as we will discuss in the next sections, it is possible to truncate this hierarchy and obtain solutions for  $G^S$  in a well-defined manner. The simplest of these solutions is the mean-field solution, which is the subject of the following section.

### A. Mean-field solution

Within the mean-field (MF) approximation, the triple-density-fluctuation propagators are assumed to be negligible in comparison with the density-density Green's functions. The MF approximation is thus obtained by dropping the nonlinear higher-order propagators to obtain a linear set of equations:

$$[-i\omega + \beta^A(\mathbf{k})]G_k^A - \alpha^B(\mathbf{k})G_k^B = -ic^A(1-c^A) \quad (3.17)$$

and

$$[-i\omega + \beta^B(\mathbf{k})]G_k^B - \alpha^A(\mathbf{k})G_k^A = ic^A c^B. \quad (3.18)$$

The diffusive pole of the Green's functions occurs at  $\omega = -i\mathbf{k} \cdot \mathbf{D} \cdot \mathbf{k}$  in the limit  $\mathbf{k} \rightarrow 0$ ,  $\omega \rightarrow 0$ . We find from (3.17) and (3.18) that

$$D_{xx} = \left[ 2c^A I^A + \frac{v(I^B M^A + I^A M^B) + 4v^2 I^A I^B}{M^A + M^B + 2v(I^A + I^B)} \right] a^2 \quad (3.19)$$

and

$$D_{yy} = \left[ \frac{v(M^A I^B + M^B I^A) + 2c^A I^A (M^A + M^B)}{M^A + M^B + 2v(I^A + I^B)} \right] b^2. \quad (3.20)$$

By symmetry, the off-diagonal elements  $D_{xy} = D_{yx} = 0$ . Equations (3.19) and (3.20) are the main results of this section. We note that the global symmetry of the diffusion constant is preserved by (3.19) and (3.20), which are symmetric under the interchange of labels  $A$  and  $B$ . When the parameters of the two sublattices are equal, i.e.,  $M^A = M^B$ ,  $I^A = I^B = I$ , and  $c^A = c^B = c/2$ , these expressions can be further simplified to correspond to our original surface model of Fig. 1 as

$$D_{xx} = I a^2 \quad (3.21)$$

and

$$D_{yy} = \frac{IM}{M + 2vI} b^2. \quad (3.22)$$

In terms of the branching ratio  $r = M/I$ , the diffusion anisotropy is then given by

$$\frac{D_{yy}}{D_{xx}} = \frac{r}{r + 2v} \left[ \frac{b}{a} \right]^2. \quad (3.23)$$

We note that even in the mean-field limit, the  $y$  component of the diffusion tensor has nontrivial coverage dependence. In the limit  $r \rightarrow \infty$ , the diffusion tensor becomes constant as required by the rigorous result in this limit.<sup>4</sup> The anisotropy ratio (3.23) also reduces to the correct geometric limit, which for the W(110) surface is  $(b/a)^2 = 2$ .<sup>6-9</sup> For values of  $r$  of unity or larger, the MF result provides a reasonably good description of the collective-diffusion case, as evidenced by a comparison in Fig. 2 of the MF results with the MC simulations. However, for smaller values of the branching ratio, the interparticle correlations play a significant role at high cover-

ages. In particular, near  $c = 1$  the MF theory gives poor results for  $D_{xx}$  and  $D_{yy}$  for  $r \lesssim 1$ , although for  $D_{yy}$  the theory is rather good for coverages  $c \lesssim 0.6-0.8$ . Nevertheless, the anisotropy ratio (3.23) is always guaranteed to be correct at  $c = 0$  and  $1$ , since blocking of intercell jumps corresponds to  $r \rightarrow \infty$  for  $c \rightarrow 1$  and thus  $D_{yy}/D_{xx} \rightarrow 2$ . Before presenting a more detailed comparison of the MF anisotropy ratio with simulations, we will study the correlation effects in detail in the next section by treating the fluctuations more accurately through a higher-order approximation.

### B. Higher-order solution

In the mean-field approximation, we neglected all higher-order terms. To study the effect of interparticle correlations in more detail, in this section we shall take into account the next-higher-order terms in the dynamic density-fluctuation expansion. This means neglecting terms only of type  $\langle\langle u_g^S u_l^{S'} u_l^{S''}; u_g^A \rangle\rangle$  (and of higher order) where all three particles are on different lattice sites. To this end we derive an equation of motion for  $G_{glg'}^{SS'}(t)$ . This can be obtained by differentiating with respect to time:

$$\begin{aligned} \frac{d}{dt} G_{glg'}^{SS'}(t) &= -2\pi i \delta(t) \langle u_g^S u_l^{S'}; u_g^A(0) \rangle \\ &\quad - 2\pi i \theta(t) \left\langle \frac{d}{dt} u_g^S \right\rangle u_l^{S'}; u_g^A(0) \rangle \\ &\quad - 2\pi i \theta(t) \left\langle u_g^S \frac{d}{dt} u_l^{S'} \right\rangle; u_g^A(0) \rangle. \end{aligned} \quad (3.24)$$

Here the fluctuations  $u^S(t)$  can be on either sublattice in each cell, giving a set of these equations for all possible combinations. To proceed further we note that the equal-time terms  $\langle\langle u_g^S(0) u_l^{S'}(0); u_g^A(0) \rangle\rangle$  can be dropped in our calculations for all four combinations of the cell indices  $g$  and  $l$ . Terms of type  $\langle\langle u_g^S(t) u_l^{S'}(t) u_l^{S''}(t); u_g^A(0) \rangle\rangle$  are neglected only if all three subscripts refer to different cells. All possible contractions leading to lower-order Green's functions which occur when the summation variable  $l'$  is identical to either  $g$  or  $l$  are taken into account.

Next, on the right-hand side of (3.24), we insert the first-order equations of types (3.1)–(3.24). To extract the diffusive behavior, we again transform the consequent set of equations into Fourier space, where the results can be written in terms of the functions  $G_k^S(\omega)$  and  $G_{\mathbf{k}-\boldsymbol{\mu},\boldsymbol{\mu}}^{SS'}(\omega)$ . The combined set of four equations of motion is compactly expressed in terms of the matrix equation

$$\underline{C} \cdot \underline{G}_{\mathbf{k}-\boldsymbol{\mu},\boldsymbol{\mu}}^{(2)} = \underline{F} \cdot \underline{G}_{\mathbf{k}}^{(1)} + \underline{R} \cdot \underline{p}_{\mathbf{k}}, \quad (3.25)$$

where matrices  $\underline{C}$ ,  $\underline{F}$ , and  $\underline{R}$  are of the order  $(4 \times 4)$ ,  $(4 \times 2)$ , and  $(4 \times 16)$ , respectively, and depend on  $\mathbf{k} - \boldsymbol{\mu}$  and  $\boldsymbol{\mu}$ . The explicit expressions for the matrix elements can be found in the Appendix. In Eq. (3.25),

$$\underline{G}_{\mathbf{k}-\mu,\mu}^{(2)} \equiv \begin{bmatrix} G_{\mathbf{k}-\mu,\mu}^{AA} \\ G_{\mathbf{k}-\mu,\mu}^{BB} \\ G_{\mathbf{k}-\mu,\mu}^{AB} \\ G_{\mathbf{k}-\mu,\mu}^{BA} \end{bmatrix}, \quad (3.26)$$

$$\underline{G}_{\mathbf{k}}^{(1)} \equiv \begin{bmatrix} G_{\mathbf{k}}^A \\ G_{\mathbf{k}}^B \end{bmatrix}, \quad (3.27)$$

and

$$\underline{\rho}_{\mathbf{k}} \equiv \begin{bmatrix} \rho_1 \\ \vdots \\ \rho_{16} \end{bmatrix}. \quad (3.28)$$

The quantities  $\rho_1$ – $\rho_{16}$  are as follows:

$$\begin{aligned} \rho_1 &= \rho_{\mathbf{k}}^{AB}(\delta_1), & \rho_2 &= \rho_{\mathbf{k}}^{AB}(\delta_2), \\ \rho_3 &= \rho_{\mathbf{k}}^{BA}(-\delta_1), & \rho_4 &= \rho_{\mathbf{k}}^{BA}(-\delta_2), \\ \rho_5 &= \rho_{\mathbf{k}}^{AA}(\delta_1), & \rho_6 &= \rho_{\mathbf{k}}^{AA}(\delta_2), \\ \rho_7 &= \rho_{\mathbf{k}}^{BB}(-\delta_1), & \rho_8 &= \rho_{\mathbf{k}}^{BB}(-\delta_2), \\ \rho_9 &= \rho_{\mathbf{k}}^{AA}(-\delta_1), & \rho_{10} &= \rho_{\mathbf{k}}^{AA}(-\delta_2), \\ \rho_{11} &= \rho_{\mathbf{k}}^{BB}(\delta_1), & \rho_{12} &= \rho_{\mathbf{k}}^{BB}(\delta_2), \\ \rho_{13} &= \rho_{\mathbf{k}}^{AB}(-\delta_1), & \rho_{14} &= \rho_{\mathbf{k}}^{AB}(-\delta_2), \\ \rho_{15} &= \rho_{\mathbf{k}}^{BA}(\delta_1), & \rho_{16} &= \rho_{\mathbf{k}}^{BA}(\delta_2). \end{aligned} \quad (3.29)$$

The equations of the motion (3.1) for the Green's functions  $\underline{G}_{\mathbf{k}}^{(1)}$  together with the equation of motion (3.25) for the Green's functions  $\underline{G}_{\mathbf{k}-\mu,\mu}^{(2)}$  constitute a closed set of equations. To proceed, we can formally solve the matrix equation (3.25) to obtain  $G_{\mathbf{k}-\mu,\mu}^{(2)}$  in terms of  $\underline{G}_{\mathbf{k}}^{(1)}$ . Using the definition (3.13) for the  $\rho_{\mathbf{k}}^{SS'}(\delta)$ 's, we can generate all of them from (3.25) by multiplying with the appropriate phase factors and integrating  $\mu$  over the first Brillouin zone. The resulting numerical values for  $\rho_1$ – $\rho_{16}$  then allow us to solve for  $\underline{G}_{\mathbf{k}-\mu,\mu}^{(2)}$  from (3.25). Finally, inserting these results back into (3.1) allows us to obtain the density-density-fluctuation Green's functions and extract the elements of the diffusion tensor in the limit  $\mathbf{k} \rightarrow 0$ ,  $\omega \rightarrow 0$ .

To avoid the complexity of the most general model, we have again solved for collective diffusion in the symmetric case where  $M^A = M^B = M$ ,  $I^A = I^B = I$ , and  $c^A = c^B = c/2$ . The elements of the diffusion tensor can be written in a simple form as

$$D_{yy} = \frac{Ir}{r+2v} b^2 f_y \quad (3.30)$$

and

$$D_{xx} = Ia^2 f_x, \quad (3.31)$$

where the *correlation factors*  $f_x$  and  $f_y$  represent corrections to the previous MF results. The diffusion anisotropy

then becomes equal to the MF result multiplied by the ratio of the correlation factors:

$$\frac{D_{yy}}{D_{xx}} = \frac{r}{r+2v} \left[ \frac{b}{a} \right]^2 \frac{f_y}{f_x}. \quad (3.32)$$

In the low-coverage limit  $c \rightarrow 0$ , we found in Sec. III A that the MF result reproduces the correct random-walk result for the diffusion tensor. For our solution to be correct, in this limit  $f_x$  and  $f_y$  must become identical to unity. In the high-coverage limit, the MF result (3.23) is again exact and the ratio  $f_y/f_x$  must approach unity. Additionally, in the limit  $r \rightarrow \infty$ , both correlation factors must again approach unity in accordance with the vanishing of all correlations.

In order to obtain the correlation factors, the numerical integrations over the Brillouin zone were done using two one-dimensional Gaussian integrals, each utilizing up to 96 Gaussian points. The reason for this high number is that the integrand is a very complicated, rapidly varying function of the wave vector. As a measure of the numerical convergence, we monitored how well the symmetry relations of Eq. (3.14) between the  $\rho$ 's were satisfied. In fact, by using the symmetry between sublattices  $A$  and  $B$ , it is possible to reduce greatly the number of independent terms needed in the calculations. For our 96 Gaussian points the symmetry relations were in general satisfied to 1 part in 1000. The numerical convergence was worst for small branching ratios and coverages close to unity, where we expect the correlations to be very strong.

In Fig. 4 we show results of comparisons of the analytical results for  $f_x$  and  $f_y$  with MC simulations, for  $r=3$  and  $\frac{1}{10}$ . For reference, we also display the MF results, which are trivially given by  $f_x \equiv f_y \equiv 1$ . We can see that the second-order solution is considerably more accurate than the MF result for  $r=3$ , but that it becomes quantitatively rather inaccurate for  $r = \frac{1}{10}$ . In particular, the second-order solution apparently fails to converge toward the correct result in the limit  $c \rightarrow 1$ . The reason for this is that the higher-order Green's functions we have neglected contain terms proportional to  $(1-c^A)$  or  $(1-c^B)$ , neither of which vanish in this limit. Physically, this means that when  $r$  diminishes, the intercell jumps cause strong multiparticle correlations to appear, which cannot be included in our higher-order solution. Thus the theoretical solution we have developed is *not* guaranteed to become exact for  $c \rightarrow 1$ .

#### IV. SUMMARY AND CONCLUSIONS

In this work we have presented a detailed theoretical study of collective diffusion in a two-step lattice-gas model. We have performed extensive random-walk MC simulations to study the behavior of the diffusion tensor and, in particular, the diffusion anisotropy in this model. Moreover, we have demonstrated that the Green's-function method of Tahir-Kheli and Elliott<sup>14</sup> can be generalized for a model of collective diffusion with two different sublattices in each cell, and the diffusion tensor

can be calculated analytically for all coverages. We note that our results for the general model of Fig. 3 can be utilized to incorporate a variety of different geometries to study other similar models of diffusion. Within the mean-field approximation, we have obtained an analytic solution which describes the diffusion anisotropy quite well for branching ratios  $r \gtrsim 1$ . We have also studied the effect of interparticle correlations in more detail by constructing a higher-order solution. Although more accurate than the MF result, this solution fails for smaller branching ratios in the high-coverage limit. In principle, it could be improved upon by taking into account even higher-order Green's functions. Unfortunately, such a solution becomes exceedingly tedious to construct. Another possibility which has been suggested<sup>15-17</sup> would be to self-consistently renormalize the existing solution to incorporate approximately the effect of the neglected

terms. Such a solution is outside the scope of the present work, however.

Our results demonstrate clearly that the experimentally observed anomalous anisotropy of collective diffusion  $D_{yy}/D_{xx} \approx 1.2$  of H adatoms on a W(110) surface<sup>8</sup> can be qualitatively explained by the symmetry breaking associated with the hourglass adsorption sites. In Fig. 5(a) we show results for the anisotropy ratio corresponding to  $r=3$ , which give  $D_{yy}/D_{xx}=1.2$  at  $c=0$ . For reference, we also show the corresponding result for  $r=\frac{1}{10}$  in Fig. 5(b). An important feature of our model is that in the regime  $c \lesssim 0.5$ , where the W(110) surface remains unreconstructed, the diffusion anisotropy is a rather slowly varying function of coverage. Furthermore, our preliminary results for the anisotropy in a model including additional adatom interactions indicate<sup>12</sup> that as long as ordered phases are not present, the results do not significantly

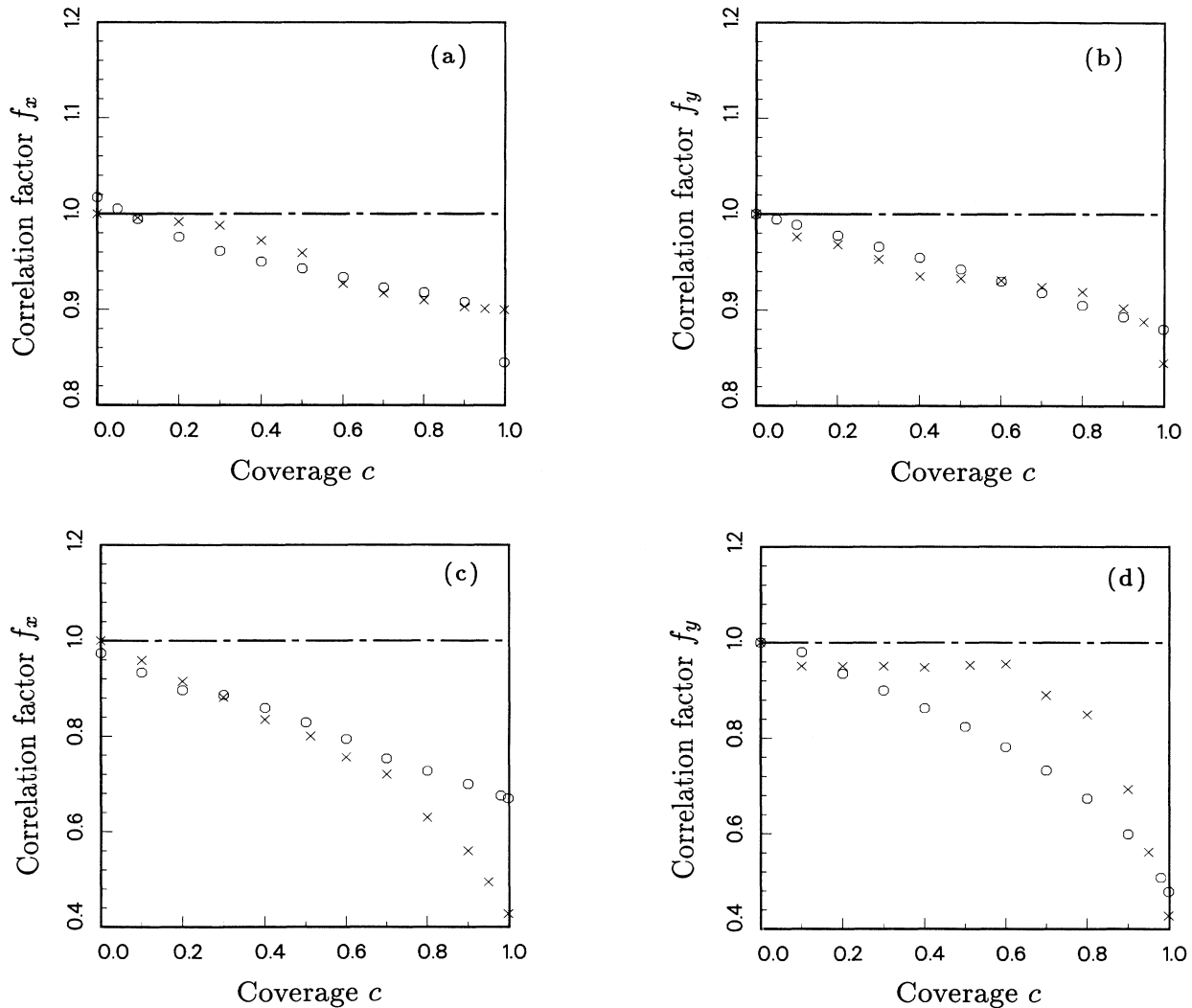


FIG. 4. Comparisons of results for the correlation factors  $f_x$  and  $f_y$  from the second-order solution of Sec. III B (circles) with MC simulations (crosses). In each case the trivial MF result  $f_x = f_y = 1$  is shown by a horizontal dashed line. (a)  $f_x$  and (b)  $f_y$  for branching ratio  $r=3$ , (c)  $f_x$  and (d)  $f_y$  for  $r=\frac{1}{10}$ . Error bars in the MC results are less than or about the size of the crosses.

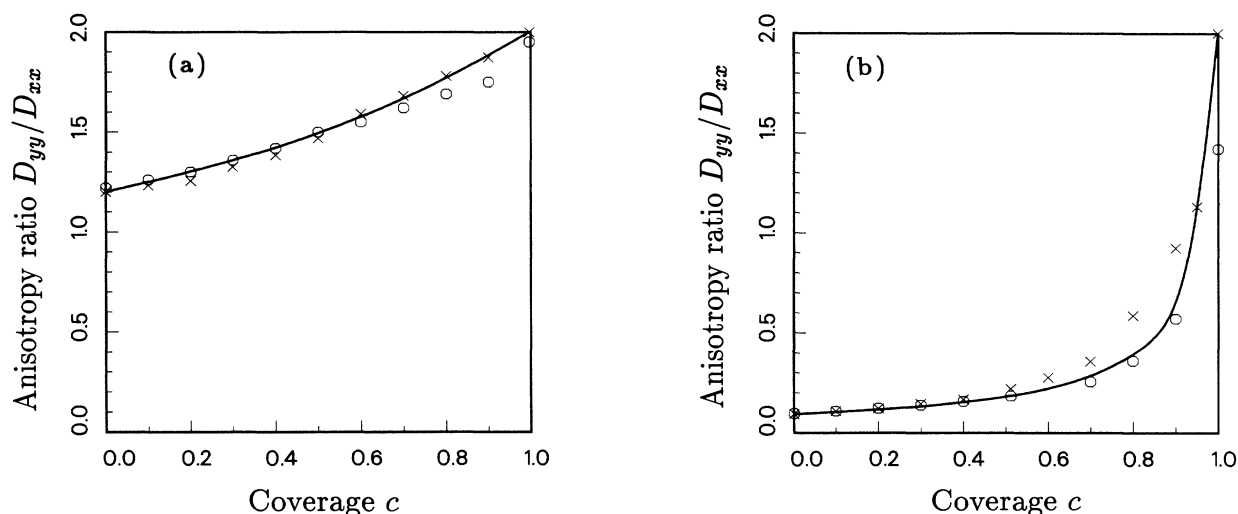


FIG. 5. Anisotropy ratio  $D_{yy}/D_{xx}$  for (a)  $r=3$  and (b)  $r=\frac{1}{10}$  corresponding to the geometry of the W(110) surface. Solid line is the MF result (3.23), while crosses denote MC simulations and circles the analytic second-order solution.

differ from those presented here. Thus we expect that even the noninteracting model studied in this work applies qualitatively to the H/W(110) system at high temperatures and low coverages.

Finally, we would like to mention an interesting connection of our lattice-gas model to percolation theory.<sup>18</sup> To this end we consider the case  $c=1-1/N$ , where all but one of the  $N$  cells on the lattice are occupied. Then the collective-diffusion tensor remains nonzero for  $r>0$ . The diffusion process occurs via the motion of a *hole* which occupies both sites of the one empty cell simultaneously. If the hole resides at a cell  $g$ , it can move to an adjacent upper (lower) cell  $g'$  if and only if the particle in that cell is in the lower  $B$  (upper  $A$ ) sublattice. One can then assign bonds between the cells, such that a bond is *closed* if the hole can jump from  $g$  to  $g'$  and is *open* otherwise. Obviously, the hole can then only move through a sequence of closed bonds. This problem is similar to current flowing in a random network of superconductors and insulators<sup>18</sup> or can also be considered as a bond percolation problem on a lattice with square geometry.<sup>19,20</sup> Namely, since the positions of the particles within each cell are random, there is on average an equal number of open and closed bonds for each fixed configuration, when intracell jumps are frozen. In this limit, which corresponds to  $r=0$ , the lattice is at its percolation threshold  $p_c=\frac{1}{2}$ , where conductivity vanishes.<sup>19</sup>

If we next consider the motion of the hole in the frozen lattice, it is well known that diffusion at this percolation threshold is anomalous.<sup>21</sup> In our model this means that  $D=0$  for  $r=0$ . However, for any *finite*  $r$ , the bonds are fluctuating and  $D>0$ . We could then expect the collective-diffusion coefficient of the particles (which is proportional to the mobility of the hole) to vanish near the percolation threshold following a power law  $D\approx r^x$

for  $r\rightarrow 0$ , where  $x$  is an unknown exponent. To study this we have performed additional simulations of the collective diffusion in the “one-hole” limit between  $r=\frac{1}{10}$  and  $\frac{1}{500}$ . Our preliminary results indicate that there indeed exists a regime where power-law behavior and a rather well-defined exponent  $x$  can be found. Fitting to our best data, we find  $x=0.47\pm 0.03$ , suggesting that  $x$  may be close to  $\frac{1}{2}$ . In this interesting limit, to clarify the relation of this “dynamical” percolation model, where the bonds are fluctuating in time, to the usual static percolation problems, more work is necessary.

#### ACKNOWLEDGMENTS

T.A-N., J.K., and S.C.Y. are supported by an ONR contract. They also acknowledge the Illinois National Center for Supercomputer Applications for allocation of computer time in Cray X-MP. R.A.T-K. thanks Institute Laue-Langevin for hospitality and support during the period this work was carried out.

#### APPENDIX

This appendix contains the explicit expressions for the matrix elements in Eq. (3.25). In the corresponding equations of motion for the second-order Green’s functions, there is a full symmetry between exchanging the sublattice indices  $A$  and  $B$  because of corresponding symmetry in the rate equations. The elements of the  $(4\times 4)$  matrix  $C$  are given by

$$\begin{aligned}
C_{1,1} &= [-i\omega + 2v^A(0) + 2c^B J^B(0) - c^A J^A(\boldsymbol{\mu}) - c^A J^A(\mathbf{k} - \boldsymbol{\mu})] , \\
C_{1,2} &= 0 , \\
C_{1,3} &= -\{[M^B - c^B J^B(0)] + vJ^B(-\boldsymbol{\mu}) + c^A J^A(\boldsymbol{\mu})\} , \\
C_{1,4} &= -\{[M^B - c^B J^B(0)] + vJ^B(-\mathbf{k} + \boldsymbol{\mu}) + c^A J^A(\mathbf{k} - \boldsymbol{\mu})\} , \\
C_{2,1} &= 0 , \\
C_{2,2} &= [-i\omega + 2v^B(0) + 2c^A J^A(0) - c^B J^B(\boldsymbol{\mu}) - c^B J^B(\mathbf{k} - \boldsymbol{\mu})] , \\
C_{2,3} &= -\{[M^A - c^A J^A(0)] + vJ^A(-\mathbf{k} + \boldsymbol{\mu}) + c^B J^B(\mathbf{k} - \boldsymbol{\mu})\} , \\
C_{2,4} &= -\{[M^A - c^A J^A(0)] + vJ^A(-\boldsymbol{\mu}) + c^B J^B(\boldsymbol{\mu})\} , \\
C_{3,1} &= \{[M^A - c^A J^A(0)] + vJ^A(-\boldsymbol{\mu}) + c^B J^B(\boldsymbol{\mu})\} , \\
C_{3,2} &= -\{[M^B - c^B J^B(0)] + vJ^A(-\mathbf{k} + \boldsymbol{\mu}) + c^A J^A(\mathbf{k} - \boldsymbol{\mu})\} , \\
C_{3,3} &= [-i\omega + v^B(0) + v^A(0) + c^A J^A(0) + c^B J^B(0) - c^A J^A(\mathbf{k} - \boldsymbol{\mu}) - c^B J^B(\boldsymbol{\mu})] , \\
C_{3,4} &= 0 , \\
C_{4,1} &= -\{[M^A - c^A J^A(0)] + vJ^A(-\mathbf{k} + \boldsymbol{\mu}) + c^B J^B(\mathbf{k} - \boldsymbol{\mu})\} , \\
C_{4,2} &= -\{[M^B - c^B J^B(0)] + vJ^B(-\boldsymbol{\mu}) + c^A J^A(\boldsymbol{\mu})\} , \\
C_{4,3} &= 0 , \\
C_{4,4} &= [-i\omega + v^B(0) + v^A(0) + c^A J^A(0) + c^B J^B(0) - c^B J^B(\mathbf{k} - \boldsymbol{\mu}) - c^A J^A(\boldsymbol{\mu})] .
\end{aligned} \tag{A1}$$

The quantities  $v^A(0) = M^A + 2vI^A$  and  $v^B(0) = M^B + 2vI^B$ .

The  $(4 \times 2)$  matrix  $F$  has the following elements:

$$\begin{aligned}
F_{1,1} &= -i\omega(1 - 2c^A) + 2[M^A(1 - c^A) + J^A(0)(v - c^A + c^A c^B)] + c^A c^B J^B(\boldsymbol{\mu}) \\
&\quad + c^A v[J^A(-\boldsymbol{\mu}) + J^A(-\mathbf{k} + \boldsymbol{\mu})] + c^A c^B J^B(\mathbf{k} - \boldsymbol{\mu}) , \\
F_{1,2} &= 2c^A[M^B - c^B J^B(0)] + c^A c^B[J^B(\boldsymbol{\mu}) + J^B(\mathbf{k} - \boldsymbol{\mu})] , \\
F_{2,1} &= 2c^B[M^A - c^A J^A(0)] + c^A c^B[J^A(\boldsymbol{\mu}) + J^A(\mathbf{k} - \boldsymbol{\mu})] , \\
F_{2,2} &= (1 - 2c^B)\{-i\omega + 2[M^B + vJ^B(0)] + 2c^A J^A(0)\} + 2c^A[M^A - c^A J^A(0)] \\
&\quad + c^A c^B[J^A(\boldsymbol{\mu}) + J^A(\mathbf{k} - \boldsymbol{\mu})] + c^B v[J^B(-\boldsymbol{\mu}) + J^B(-\mathbf{k} + \boldsymbol{\mu})] , \\
F_{3,1} &= \{i\omega c^B - c^B[v^A(0) + v^B(0) + c^A J^A(0) + c^B J^B(0)] - [M^A - c^A J^A(0)](1 - 2c^A)\} \\
&\quad + v c^B J^A(-\boldsymbol{\mu}) - c^A(1 - c^A)J^A(\mathbf{k} - \boldsymbol{\mu}) - c^B(1 - c^B)J^B(\boldsymbol{\mu}) , \\
F_{3,2} &= \{i\omega c^A - c^A[v^A(0) + v^B(0) + c^A J^A(0) + c^B J^B(0)] - [M^B - c^B J^B(0)](1 - 2c^B)\} \\
&\quad + v c^A J^B(-\mathbf{k} + \boldsymbol{\mu}) - c^A(1 - c^A)J^A(\mathbf{k} - \boldsymbol{\mu}) - c^B(1 - c^B)J^B(\boldsymbol{\mu}) , \\
F_{4,1} &= \{i\omega c^B - c^B[v^A(0) + v^B(0) + c^A J^A(0) + c^B J^B(0)] - [M^A - c^A J^A(0)](1 - 2c^A)\} \\
&\quad + v c^B J^A(-\mathbf{k} + \boldsymbol{\mu}) - c^B(1 - c^B)J^B(\mathbf{k} - \boldsymbol{\mu}) - c^A(1 - c^A)J^A(\boldsymbol{\mu}) , \\
F_{4,2} &= \{i\omega c^A - c^A[v^A(0) + v^B(0) + c^A J^A(0) + c^B J^B(0)] - [M^B - c^B J^B(0)](1 - 2c^B)\} \\
&\quad + v c^A J^B(-\boldsymbol{\mu}) - c^B(1 - c^B)J^B(\mathbf{k} - \boldsymbol{\mu}) - c^A(1 - c^A)J^A(\boldsymbol{\mu}) .
\end{aligned} \tag{A2}$$

For the  $(4 \times 16)$  matrix  $R$ , all elements appear in pairs. The elements  $R_{i,2j}$  ( $i = 1, 2, 3, 4; j = 1, 2, 3, \dots, 8$ ), with an even second index, follow from the preceding elements  $R_{i,2j-1}$  simply by letting  $\delta_1 \rightarrow \delta_2$ . For clarity, this is demonstrated below for the pair  $R_{1,1}$  and  $R_{1,2}$ :

$$\begin{aligned} R_{1,1} &= -vI^B - c^A I^A + c^A (I^B - I^A) e^{i\mu \cdot \delta_1}, \\ R_{1,2} &= R_{1,1}(\delta_1 \rightarrow \delta_2), \\ R_{1,3} &= -(vI^B + c^A I^A) e^{ik \cdot \delta_1} - c^A (I^B - I^A) e^{i\mu \cdot \delta_1}, \\ R_{1,5} &= -c^A I^A + vI^A e^{-i\mu \cdot \delta_1}, \\ R_{1,7} &= c^A I^B e^{i\mu \cdot \delta_1}, \\ R_{1,9} &= vI^A e^{i\mu \cdot \delta_1} - c^A I^A e^{ik \cdot \delta_1}, \\ R_{1,11} &= c^A I^B e^{-i\mu \cdot \delta_1}, \\ R_{1,13} &= c^B I^B e^{i\mu \cdot \delta_1}, \\ R_{1,15} &= c^B I^B e^{-i\mu \cdot \delta_1}, \\ R_{2,1} &= c^B (I^A - I^B) e^{-i\mu \cdot \delta_1} - (vI^A + c^B I^B) e^{-ik \cdot \delta_1}, \\ R_{2,3} &= +c^B (I^A - I^B) e^{i\mu \cdot \delta_1} - c^B I^B - vI^A, \\ R_{2,5} &= c^B I^A e^{-i\mu \cdot \delta_1}, \\ R_{2,7} &= -c^B I^B + vI^B e^{i\mu \cdot \delta_1}, \\ R_{2,9} &= c^B I^A e^{i\mu \cdot \delta_1}, \\ R_{2,11} &= -c^B I^B e^{-ik \cdot \delta_1} + vI^B e^{-i\mu \cdot \delta_1}, \end{aligned}$$

$$\begin{aligned} R_{2,13} &= c^A I^A e^{i\mu \cdot \delta_1}, \\ R_{2,15} &= c^A I^A e^{-i\mu \cdot \delta_1}, \\ R_{3,1} &= [(c^A - 2c^B)I^A + (c^B - 2c^A)I^B] e^{-i\mu \cdot \delta_1}, \\ R_{3,3} &= 0, \\ R_{3,5} &= (2c^A - 1 - c^B)I^A e^{-i\mu \cdot \delta_1}, \\ R_{3,7} &= -(1 - c^A)I^B e^{ik \cdot \delta_1}, \\ R_{3,9} &= (c^B - 1)I^A, \\ R_{3,11} &= (2c^B - 1 - c^A)I^B e^{-i\mu \cdot \delta_1}, \\ R_{3,13} &= -(c^B I^B + c^A I^A e^{ik \cdot \delta_1}), \\ R_{3,15} &= 0, \\ R_{4,1} &= 0, \\ R_{4,3} &= [(c^B - 2c^A)I^B + (c^A - 2c^B)I^A] e^{i\mu \cdot \delta_1}, \\ R_{4,5} &= -(1 - c^B)I^A e^{-ik \cdot \delta_1}, \\ R_{4,7} &= (2c^B - 1 - c^A)I^B e^{i\mu \cdot \delta_1}, \\ R_{4,9} &= (2c^A - 1 - c^B)I^A e^{i\mu \cdot \delta_1}, \\ R_{4,11} &= (c^A - 1)I^B, \\ R_{4,13} &= 0, \\ R_{4,15} &= -(c^A I^A + c^B I^B e^{-ik \cdot \delta_1}). \end{aligned} \tag{A3}$$

\*Permanent address: Department of Physics, Tampere University of Technology, P. O. Box 527, SF-33101 Tampere, Finland.

<sup>1</sup>See, e.g., K. W. Kehr, R. Kutner, and K. Binder, *Phys. Rev. B* **23**, 4391 (1981).

<sup>2</sup>K. W. Kehr and K. Binder, in *Applications of the Monte Carlo Method in Statistical Physics*, edited by K. Binder (Springer-Verlag, New York, 1987), and references cited therein.

<sup>3</sup>R. A. Tahir-Kheli (unpublished).

<sup>4</sup>R. Kutner, *Phys. Lett.* **81A**, 239 (1981).

<sup>5</sup>R. Gomer, *Rep. Prog. Phys.* **53**, 917 (1990).

<sup>6</sup>M. Tringides and R. Gomer, *Surf. Sci.* **166**, 419 (1986); **166**, 440 (1986).

<sup>7</sup>J. Kjoll, T. Ala-Nissila, and S. C. Ying, *Surf. Sci.* **218**, L476 (1989).

<sup>8</sup>M. Tringides and R. Gomer, *Surf. Sci.* **155**, 254 (1985).

<sup>9</sup>T. Ala-Nissila and S. C. Ying, *Surf. Sci. Lett.* **235**, L341 (1990).

<sup>10</sup>J. W. Chung, P. Estrup, and S. C. Ying, *Phys. Rev. Lett.* **56**, 749 (1986); D. Sahu, J. M. Kosterlitz, and S. C. Ying, in *The Structure of Surfaces II*, edited by J. F. Van der Veer and M. A. Van Hove (Springer-Verlag, New York, 1988).

<sup>11</sup>T. Ala-Nissila, J. Kjoll, S. C. Ying, and R. A. Tahir-Kheli, following paper, *Phys. Rev. B* **44**, 2133 (1991).

<sup>12</sup>J. Kjoll, T. Ala-Nissila, and S. C. Ying (unpublished).

<sup>13</sup>C. H. Mak, H. C. Anderson, and S. M. George, *J. Chem. Phys.* **88**, 4052 (1988).

<sup>14</sup>R. A. Tahir-Kheli and R. J. Elliott, *Phys. Rev. B* **27**, 844 (1983).

<sup>15</sup>R. A. Tahir-Kheli, *Phys. Rev. B* **27**, 6072 (1983); R. A. Tahir-Kheli and N. El-Meshad, *ibid.* **32**, 6166 (1985).

<sup>16</sup>P. C. W. Holdsworth and R. J. Elliott, *Philos. Mag. A* **54**, 601 (1986).

<sup>17</sup>R. A. Tahir-Kheli, P. C. Holdsworth, and R. J. Elliott (unpublished); R. A. Tahir-Kheli (unpublished).

<sup>18</sup>D. Stauffer, *Introduction to Percolation Theory* (Taylor and Francis, Philadelphia, 1985).

<sup>19</sup>J. W. Essam, in *Phase Transitions and Critical Phenomena*, edited by M. S. Green and C. Domb (Academic, New York, 1972), Vol. 2.

<sup>20</sup>An additional complication for the motion of the hole is that in our model, some of the assigned bonds between adjacent cells are *directional*; i.e. they may only "conduct" in one direction.

<sup>21</sup>D. Ben-Avraham and S. Havlin, *J. Phys. A* **15**, L691 (1982); Y. Gefen, A. Aharony, and S. Alexander, *Rev. Lett.* **50**, 77 (1983); B. O'Shaughnessy and I. Procaccia, *ibid.* **54**, 455 (1985); Th. M. Nieuwenhuizen, P. F. J. van Velthoven, and M. H. Ernst, *ibid.* **57**, 2477 (1986).